MATERIALS SCIENCE

A constant current triboelectric nanogenerator arising from electrostatic breakdown

Di Liu[1,2]*, Xing Yin[1,2]*, Hengyu Guo[1,3]*, Linglin Zhou[1,2], Xinyuan Li[1,2], Chunlei Zhang[1,2], Jie Wang[1,2]†, Zhong Lin Wang[1,2,3]†

Copyright © 2019 The Authors, some rights reserved; exclusive licensee American Association for the Advancement of Science. No claim to original U.S. Government Works. Distributed under a Creative Commons Attribution NonCommercial License 4.0 (CC BY-NC).

In situ conversion of mechanical energy into electricity is a feasible solution to satisfy the increasing power demand of the Internet of Things (IoTs). A triboelectric nanogenerator (TENG) is considered as a potential solution via building self-powered systems. Based on the triboelectrification effect and electrostatic induction, a conventional TENG with pulsed AC output characteristics always needs rectification and energy storage units to obtain a constant DC output to drive electronic devices. Here, we report a next-generation TENG, which realizes constant current (crest factor, ~1) output by coupling the triboelectrification effect and electrostatic breakdown. Meanwhile, a triboelectric charge density of 430 μC m^{-2} is attained, which is much higher than that of a conventional TENG limited by electrostatic breakdown. The novel DC-TENG is demonstrated to power electronics directly. Our findings not only promote the miniaturization of self-powered systems used in IoTs but also provide a paradigm-shifting technique to harvest mechanical energy.

INTRODUCTION

In recent years, intensive work has been dedicated to converting environmental energy into electricity to meet modern society's demand of a clean and sustainable power source (*1*–*5*). Harvesting of environmental mechanical energy as an eco-friendly energy generation method is particularly a promising solution and plays an increasingly important role in driving wearable electronics and sensor networks in the Internet of Things (IoTs) (*6*–*9*). Owing to its wide distribution and sufficient availability, mechanical energy harvesting has attracted extensive attention and many mechanisms have been explored, such as electromagnetic generators (EMGs) (*10*, *11*), piezoelectric nanogenerators (PENGs) (*4*, *5*, *12*, *13*), and triboelectric nanogenerators (TENGs) (*14*–*16*), to name a few. Among them, EMGs, based on Faraday's law of electromagnetic induction, are suitable for large-scale power generation. PENGs can convert tiny physical deformation into electricity to self-power small-scale devices (*4*, *17*). On the basis of the triboelectrification effect and electrostatic induction, TENGs have been demonstrated as a cost-effective, clean, and sustainable strategy to convert mechanical energy into electricity (*18*–*20*) with its comprehensive advantages: lightweight, small size, a wide choice of materials, and high efficiency even at low frequencies (*21*–*26*).

The output of conventional TENGs has two built-in characteristics (i.e., AC consisted of pulse series). First, it requires a rectifier to get a DC output, such as the full-wave rectifier, a rotary rectifier bridge (*27*), a double-wheel design (*28*), or a multiphase rotation-type structure (*29*), which takes away its portability advantage. In addition, when powered by AC, some applications require electromagnetic shielding, such as sensor integration, which will reduce integration degree (*30*). Second, the pulsed output results in a very high crest factor, which is a key metric to output instability defined as the ratio of the peak value to the root mean square value. This seriously influences its performance in energy storage and powering electronics (*29*), where constant DC input is preferred. Very recently, a continuous DC output has been realized using the sliding Schottky nanocontact technique; however, the output voltage is too low (~ 8 mV) to drive electronics directly (*31*).

To address these issues, a paradigm-shifting TENG is invented to directly generate constant DC by coupling the triboelectrification effect and electrostatic breakdown. Its charge density reaches 430 μC m^{-2}, which is much higher than that of a conventional TENG limited by air breakdown. Its voltage increases with load, up to 750 V in our experiments, making it a possible replacement for batteries in many applications because it provides excellent constant current power; moreover, it does not contribute to environmental pollution and does not incur a recycling cost. The novel DC-TENG demonstrates effective mechanical energy harvesting to power electronics solely or to directly charge an energy storage unit simultaneously, which can greatly accelerate the miniaturization of self-powered systems used in wearable electronics and IoTs.

RESULTS

Working principle of DC-TENG

Triboelectrification, which refers to the charge transfer between two surfaces in contact, is the principle behind natural phenomena such as the amber effect and lightning (Fig. 1A, i). Lightning is caused by the electrostatic charge accumulation resulting from the triboelectric effect in a thundercloud and electrostatic breakdown in air, which releases huge amounts of energy (several billions of joules) that are very difficult to harvest. TENG, based on the triboelectrification effect and electrostatic induction, was invented to harvest mechanical energy from the ambient environment (Fig. 1A, ii) (*18*). However, a very high electrostatic field will be built in TENG, which also leads to air breakdown, and will therefore result in unwanted charge quantity loss and, consequently, quadratic loss in output power (*32*, *33*). The charge quantity loss can be roughly estimated with its charge density gap in air and vacuum. With a 50-μm polytetrafluoroethylene (PTFE) film as the triboelectric layer, 240 μC m^{-2} is

[1]Beijing Institute of Nanoenergy and Nanosystems, Chinese Academy of Sciences, Beijing 100083, P. R. China. [2]College of Nanoscience and Technology, University of Chinese Academy of Sciences, Beijing 100049, P. R. China. [3]School of Materials Science and Engineering, Georgia Institute of Technology, Atlanta, GA 30332, USA.
*These authors contributed equally to this work.
†Corresponding author. Email: wangjie@binn.cas.cn (J.W.); zhong.wang@mse.gatech.edu (Z.L.W.)

Downloaded from http://advances.sciencemag.org/ on March 31, 2021

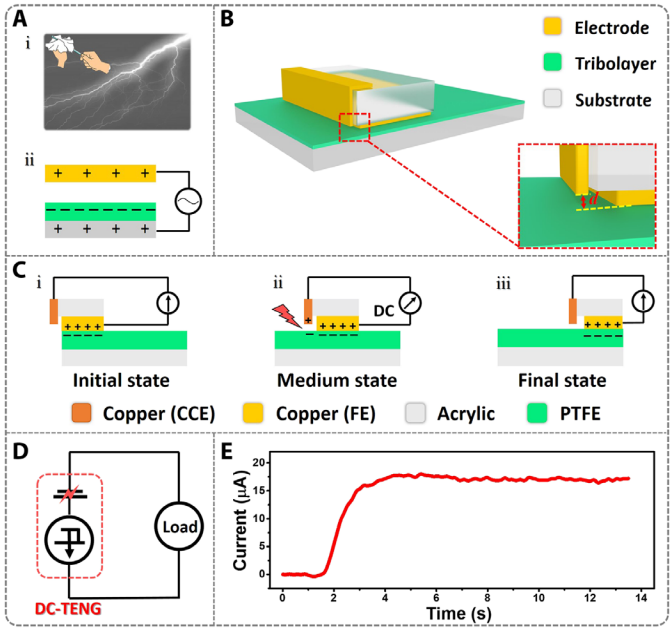

Fig. 1. Working principle of the DC-TENG. (**A**) (i) Phenomenon of the triboelectrification effect and electrostatic breakdown (lightning) in nature. (ii) Working mechanism of a conventional TENG. (**B**) A schematic illustration of the sliding mode DC-TENG. (**C**) Working mechanism of the sliding mode DC-TENG in full cyclic motion. (**D**) Equivalent circuit model of the DC-TENG. (**E**) Constant current output of the DC-TENG.

the theoretical upper limit in air (*33*–*35*), but 1003 μC m^{-2} has been achieved in vacuum (*36*), where a dominant part is wasted because of air breakdown.

To harvest energy during electrostatic breakdown, a next-generation DC-TENG is designed via the triboelectrification effect and by inducing artificial lightning. It is composed of a charge collecting electrode (CCE), a frictional electrode (FE), and a triboelectric layer (Fig. 1B). The CCE layer is fixed on the side of a sliding acrylic substrate, with a subtle distance to the triboelectric layer, which is a PTFE layer attached to another acrylic sheet. Here, both CCE and FE are copper electrodes.

The working mechanism of DC-TENG based on dielectric breakdown is illustrated in Fig. 1C. In the initial state, the FE is in left alignment with the PTFE film and is in contact with PTFE, and there are positive charges on the FE and negative charges on PTFE caused by the triboelectrification effect (Fig. 1C, i). Because the PTFE film is an electret, it can hold a quasi-permanent electric charge. Thus, in the medium state when the slider moves forward under an external force, a very high electrostatic field is built between the CCE and the negatively charged PTFE film. As long as it exceeds the dielectric strength of the air between them, whose value is approximately 3 kV/mm from Paschen's law, it can cause the nearby air to partially ionize and begin conducting. This will result in electrons flowing from the PTFE to the CCE, thus reducing the potential difference (Fig. 1C, ii); i.e., the CCE is rationally placed to induce air breakdown, creating artificial lightning. Instead of allowing air breakdown to happen spontaneously and having its energy untapped in a conventional TENG, the CCE effectively collects these charges. The discharging process will continue until FE is in right alignment with the PTFE film (Fig. 1C, iii). Briefly, the electrons on the FE transfer to PTFE via the triboelectrification process and then they transport to the CCE via electrostatic breakdown and ultimately to the FE via an external circuit. Because the inner flow direction of electrons is fixed from the FE to the PTFE film and then to the CCE, the output electrons will also be in a single direction, i.e., from the CCE to the FE. When the slider moves backward to the initial state, no current flows in the external circuit because there is not enough potential difference across the CCE and the PTFE film for dielectric breakdown to occur. Thus, cyclic DC can be produced by periodically sliding the slider. The detailed working mechanism of the sliding mode DC-TENG during the first cycle is shown in fig. S1 and note S1.

The physics model of the new DC-TENG is made up of an electric charge source and a broken-down capacitor composed of the CCE and PTFE film, as its equivalent circuit briefly demonstrates in Fig. 1D. The DC resulted from the unidirectional dielectric breakdown of the capacitor producing ongoing conduction current (Fig. 1E). It is different from a conventional TENG, whose paradigm is a variable capacitor initially charged by triboelectrification and generating AC pluses by electrostatic induction (figs. S2 and S3 and note S2). In other words, the charge quantity harvested by the DC-TENG via dielectric breakdown is a complement of charge quantity harvested by a conventional TENG via electrostatic induction, and their union is the whole triboelectric charge quantity. In this work, we found that the former is larger than the latter. This new paradigm is easy to generalize via other dielectric breakdowns and can be further considered as a prototype of lightning energy harvesting. The detailed mechanism and the precise theoretical model need to be investigated in future work.

Output performance of the sliding mode DC-TENG

On the basis of the proposed mechanism, two modes of DC-TENG are designed: the sliding mode and the rotary mode. Figure 2A shows a photograph of the stator and the slider (inset) of the sliding mode DC-TENG. Figure 2B shows a SEM image of nanowires on the surface of PTFE. When the slider moves along the electrification layer, the corona discharge phenomenon of air breakdown between PTFE and the CCE is captured (Fig. 2C), which is solid evidence of the air breakdown occurrence during device operation. We also measured the surface potential of PTFE to demonstrate that some electrostatic charges are discharged by electrostatic breakdown (fig. S4). Figure 2 (D to F) plots the short-circuit current (I_{SC}), transferred charges, and open-circuit voltage (V_{OC}) of the sliding mode DC-TENG. The I_{SC} and V_{OC} are about 1.05 μA and 14.2 V at an acceleration of 6 m s^{-2}. The transferred charge during one cycle is up to 157 nC. These all exhibit good DC output characteristics. For the sliding motion, the I_{SC} increases with acceleration, from 0.375 μA at 1 m s^{-2} to 1.05 μA at 6 m s^{-2} (Fig. 2G). The V_{OC} also increases correspondingly, from 4.8 to 14.2 V (Fig. 2I). Note that the transferred charge is invariant at different accelerations (Fig. 2H) because it is determined by the collected charge area after triboelectrification, while the I_{SC} and V_{OC} are relevant with the charge transfer rate. When the slider moves at a constant speed, the I_{SC} remains stable, such as 0.1 μA at a speed of 0.05 m s^{-1} and 0.77 μA at a speed of 0.4 m s^{-1} (Fig. 2J). The V_{OC} also increases with velocity from 1.08 to 9.6 V (Fig. 2K). The transferred charge of 195 nC is barely affected by velocity during one cycle (fig. S5).

Furthermore, the charge density of the DC-TENG is compared with that of a conventional sliding mode TENG under the same conditions.

Downloaded from http://advances.sciencemag.org/ on March 31, 2021

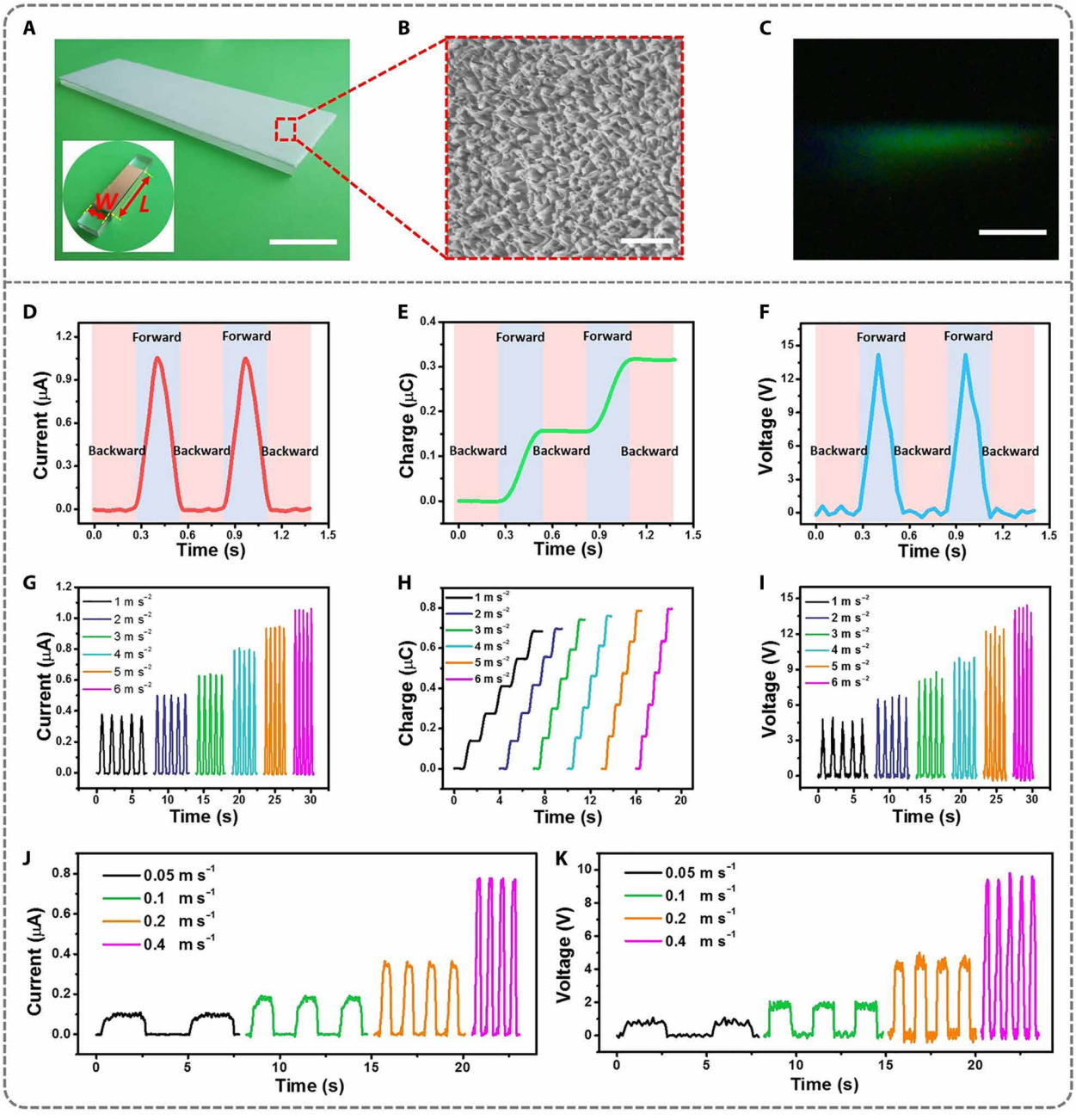

Fig. 2. Output performance of the sliding mode DC-TENG. (**A**) Photographs of the stator and the slider (inset) of the sliding mode DC-TENG (*W* is the width of the FE and *L* is the length of CCE; scale bar, 3 cm). (**B**) Scanning electron microscopy (SEM) image of nanowires on the surface of PTFE. Scale bar, 1 μm. A larger surface curvature results in an ultrahigh electric field, which is easier to air breakdown. (**C**) Phenomenon of air discharge in this paper. Scale bar, 1 cm. (**D**) Short-circuit current, (**E**) transferred charges, and (**F**) open-circuit voltage of the sliding mode DC-TENG. (**G**) Short-circuit current, (**H**) transferred charges, and (**I**) open-circuit voltage of the sliding mode DC-TENG at different accelerations. (**J**) Short-circuit current and (**K**) open-circuit voltage of the sliding mode DC-TENG at different velocities.

By using the PTFE film and nitrile as the triboelectric materials, the charge density reaches 330 μC m^{-2} (fig. S6), which is obviously higher than that of a conventional sliding TENG (~70 μC m^{-2}), which is limited by air breakdown. After introducing nanostructures on the surface of the PTFE film via the inductively coupled plasma process to produce reactive ion etching, the charge density is increased to 430 μC m^{-2} (fig. S7), which is equivalent to a sixfold enhancement. If calculated by the area of the FE, the value is up to 2150 μC m^{-2}; that is, a 30-fold enhancement is obtained (table S1).

The gap between the CCE and PTFE has a great effect on the electric field with the potential difference being constant, which is an extremely important parameter to optimize the output performance of the DC-TENG. From fig. S8, the I_{SC} decreases with an increase in gap. This is due to the gradually decreased electric field as the gap increases, resulting in fewer electrons for air breakdown (note S3).

In addition, we fabricated a sliding mode DC-TENG with two CCEs at both ends of the slider. The working mechanism of this

Downloaded from http://advances.sciencemag.org/ on March 31, 2021

structure is similar to that of the DC-TENG with one CCE, and its details are shown in fig. S9. Its I_{SC} and transferred charges are briefly presented in note S4 and fig. S10. There is a current output in the external circuit when the slider moves backward, and the amount of transferred charges is doubled during one cycle, compared to the DC-TENG with a single CCE. It indicates that its output performance can be rapidly enhanced by simple structure optimization.

Furthermore, the influence of the FE width (W) in the DC-TENG on the output characteristics is evaluated (note S5 and fig. S11). The transferred charge and I_{SC} increase with the decrease in the FE width because of the increase in contact intimacy. In particular, they are substantially enhanced when the width is smaller than 5 mm, indicating that the output power can be further improved by decreasing the volume of the DC-TENG and parallelizing the connection of multiple DC-TENGs (fig. S12). It provides an easy and efficient way to improve the output performance of the DC-TENG to drive electronic devices requiring more power. As for the length (L) of the CCE, fig. S13 shows that a higher output is obtained with a longer CCE. Because the sliding area is directly proportional to the CCE length when the sliding distance remains constant, more charges will be obtained with larger frictional area. Furthermore, we also tested the long-term output current of the DC-TENG. After 3000 s of repeated sliding, the output current nearly remains constant, thus confirming its excellent stability (fig. S14).

Output performance of a rotary mode DC-TENG

Parallel multiple DC-TENGs are realized by a radially arrayed rotary mode DC-TENG. Its structure is shown in Fig. 3A, which

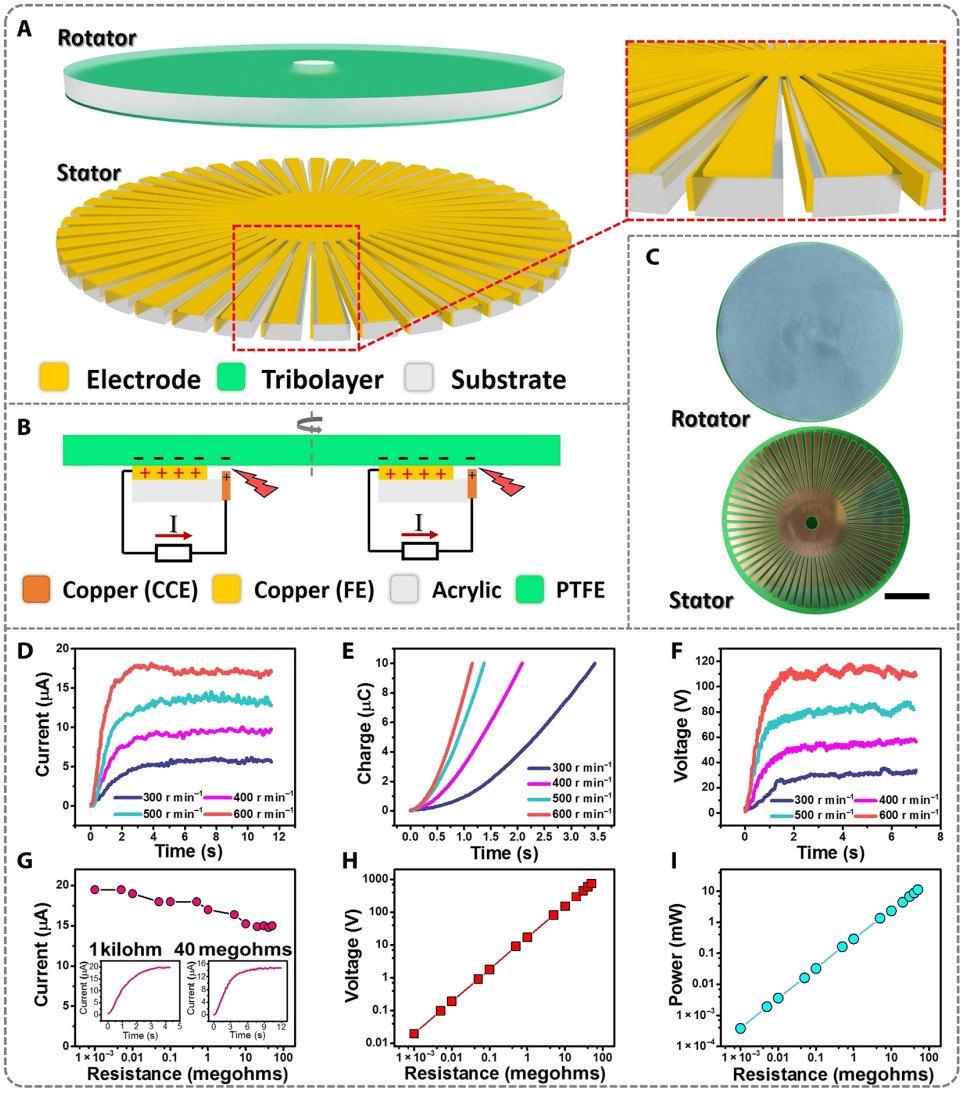

Fig. 3. Working mechanism and output performance of the rotary mode DC-TENG. (**A**) Structural design of the rotary mode DC-TENG. Inset shows a zoomed-in illustration of its stator. (**B**) Working mechanism of the rotary mode DC-TENG. (**C**) Photographs of the fabricated rotary mode DC-TENG. Scale bar, 5 cm. (**D**) Short-circuit current, (**E**) transferred charges, and (**F**) open-circuit voltage of the rotary mode DC-TENG at different rotation rates (300, 400, 500, and 600 r min^{-1}). (**G**) Output current of the rotary mode DC-TENG with various resistances. Inset shows the detailed output current at 1 kilohm and 40 megohms. (**H**) Output voltage and (**I**) power of the rotary mode DC-TENG with various resistances.

Downloaded from http://advances.sciencemag.org/ on March 31, 2021

consists of a stator and a rotator. The stator is composed of many sectors, each unit of which is similar to that of a sliding mode DC-TENG. All the FEs and CCEs are connected. Electricity generation relies on the relative rotation between the rotator and the stator (Fig. 3B), which is equivalent to connect many sliding mode DC-TENGs in parallel. Figure 3C shows a photograph of the rotator and the stator.

To reveal the relationship between rotation rate and performance, we tested the value of output current, speed of charge transfer, and V_{OC}. When the rotary motor rotates stably, the said values are 5.79 μA, 5.39 μC s^{-1}, and 50 V at 300 r min^{-1} and 17.00 μA, 17.81 μC s^{-1}, and 115 V at 600 r min^{-1}, respectively (Fig. 3, D to F, and fig. S15), which enables the motor to directly drive electronics and effectively charge energy storage units simultaneously. The crest factor is very close to 1, and the average charge is close to the average value of a steady current, both of which indicate approximately constant current output characteristics (tables S2 and S3 and note S6). Applying an external load, the output current almost remains stable and the output voltage increases correspondingly, indicating approximately constant current output characteristics again (Fig. 3G). The corresponding output voltage and power are shown in Fig. 3 (H and I), which nearly increase with the load linearly, from 0.02 to 750 V and from 0.38 μW to 10 mW, respectively. Because output current (I) remains nearly constant with the increase in load resistance, the output power of the DC-TENG ($P = I^2R$) has a linear relationship under load resistances (R). Compared with a conventional TENG, the output current gradually decreases with an increase in load resistance, wherefore the output power increases with the load resistances and then decreases.

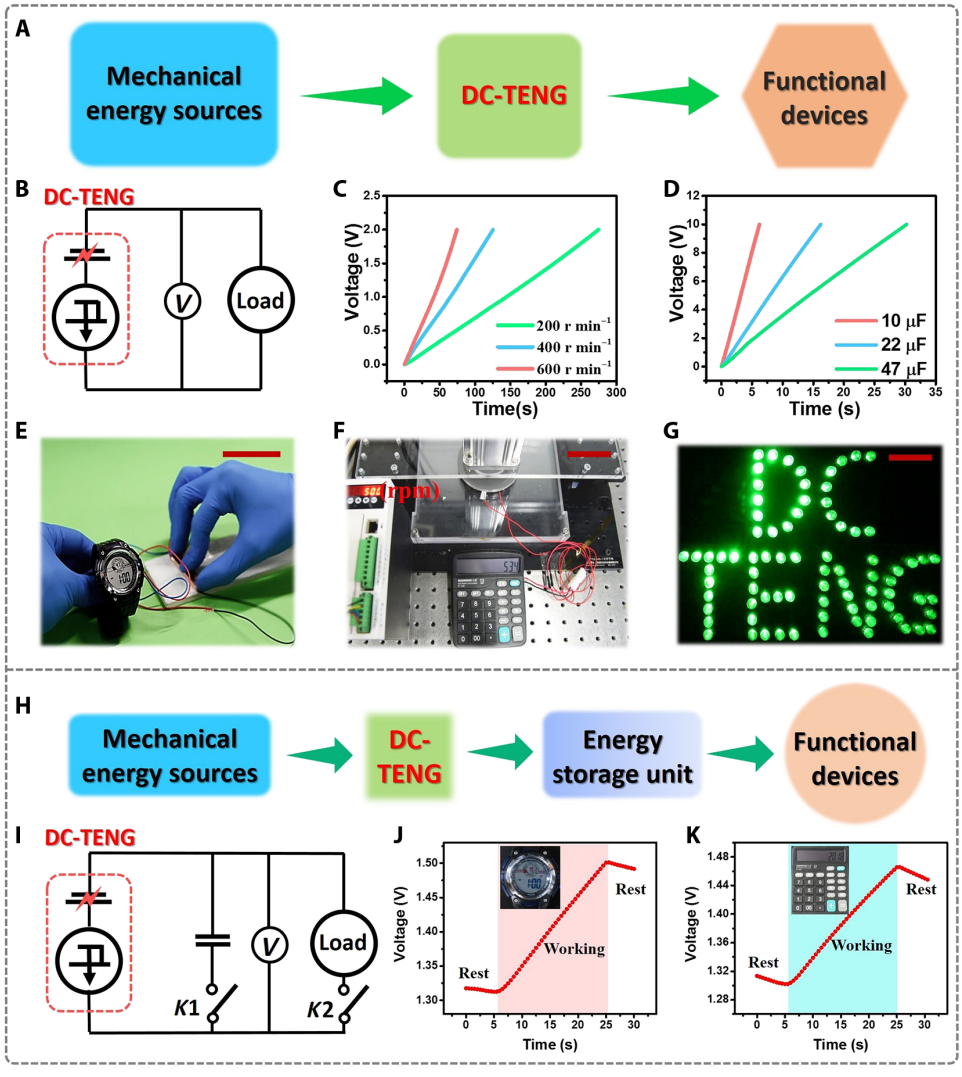

Fig. 4. Application of the DC-TENG to drive electronic devices. (**A**) System diagram and (**B**) circuit diagram of a DC-TENG–based self-powered system to power electronics directly. (**C**) Measured voltage of a capacitor (470 μF) charged by a rotary mode DC-TENG at different rotation rates. (**D**) Charging curves of capacitors with various capacitance charged by a rotary mode DC-TENG at a rotating speed of 500 r min^{-1}. (**E**) Photograph of a watch directly driven by a sliding mode DC-TENG. (**F**) Photograph of a scientific calculator directly driven by a rotary mode DC-TENG. (**G**) Photograph of 81 LEDs with stable luminance powered by a rotary mode DC-TENG. (**H**) System diagram and (**I**) circuit diagram of the self-powered system to power electronics with energy storage units. (**J**) Charging curves of the capacitor when the watch is driven by a rotary mode DC-TENG simultaneously. (**K**) Charging curves of the capacitor when the scientific calculator is driven by a rotary mode DC-TENG simultaneously. Scale bars, 5 cm. Photo credit for (E), (F), (G), (J), and (K): X. Yin, Chinese Academy of Sciences.

Downloaded from http://advances.sciencemag.org/ on March 31, 2021

Application of DC-TENG to drive electronic devices

The ability to generate continuous DC output enables the novel DC-TENG to not only charge energy storage devices directly but also power electronics solely and directly without a rectifier unit. Figure 4A shows a diagram of the DC-TENG–based self-powered system to drive electronics directly, with the corresponding circuit diagram shown in Fig. 4B. Figure 4C shows the voltage curves of a capacitor with a capacitance of 470 μF charged directly by a rotary mode DC-TENG without a rectifier at different rotation rates (200, 400, and 600 r min^{-1}). The charging rate increases with the rotation rates, and the capacitor can be charged to 2 V within 70 s in 600 r min^{-1}. Figure 4D depicts charging curves of different capacitors (10, 22, and 47 μF) charged by a rotary mode DC-TENG at a speed of 500 r min^{-1}, where the 10-μF capacitor can be instantly charged to 10 V within 6 s. Furthermore, an electronic watch is directly driven by a sliding mode DC-TENG (Fig. 4E and movie S1). A scientific calculator can also be driven by a rotary mode DC-TENG with a diameter of 10 cm and with a rotation rate of 500 r min^{-1} (Fig. 4F and movie S2). A light-emitting diode (LED) bulb array (rated power 0.75 W × 81) can also be lit up by the rotary mode DC-TENG with a rotation rate of 500 r min^{-1} (Fig. 4G and movie S3). Unlike LEDs driven by the conventional TENG, these LEDs remain at constant luminance without flashing lights.

The DC-TENG can also act as a power source directly driving electronics and charging energy storage devices simultaneously by integrating with an energy storage unit to build a self-powered system (Fig. 4H). Taking the capacitor as the storage unit, the circuit diagram of the system is presented in Fig. 4I, where the DC-TENG and a capacitor are connected directly. The voltage of the capacitor is monitored by a voltmeter. As shown in Fig. 4J, the voltage of the capacitor decreases when the capacitor powers the electronic watch alone at first, and the equivalent input current (I_e) of the electronic watch is calculated as 2.05 μA (note S7). While the rotary mode DC-TENG operates, the voltage of the capacitor increases, indicating that its output energy allows the DC-TENG to power the device and charge the capacitor simultaneously and sustainably with a charging current of 10.17 μA. To drive a scientific calculator with a higher power consumption, the DC-TENG continues to exhibit excellent output, and the charging current of the capacitor is 8.71 μA (Fig. 4K).

DISCUSSION

In summary, we have achieved the conversion of mechanical energy into constant output current by designing a next-generation TENG based on the triboelectrification effect and electrostatic breakdown. A sliding mode DC-TENG and a rotary mode DC-TENG were fabricated to demonstrate the new mechanism. In the sliding mode DC-TENG, its charge density reaches 430 μC m^{-2}, which is much higher than the value of a conventional TENG limited by air breakdown. In the rotary mode DC-TENG, an I_{SC} of 15 μA and a V_{OC} of 750 V are attained. The crest factor of this TENG is close to 1, indicating that a constant current output is obtained. Moreover, the novel DC-TENG is demonstrated to be an effective strategy in harvesting mechanical energy to directly power electronics or to charge an energy storage unit without any rectifier. Our findings not only promote the miniaturization of self-powered systems used in wearable electronics and sensor networks in IoTs but also provide a paradigm-shifting technique for TENG to effectively convert mechanical energy into electricity. Furthermore, it can be further considered as a prototype of lightning energy harvesting.

MATERIALS AND METHODS

Fabrication of the sliding mode DC-TENG

Stator: (i) Cut a rectangle acrylic sheet as the substrate with dimensions of 20 cm (length) by 5 cm (width) by 5 mm (thickness) using a laser cutter (PLS6.75, Universal Laser Systems). (ii) To achieve a flexible and fragmental structure, adhere a piece of foam between the substrate and the PTFE film with the same size, 20 cm by 5 cm. Use PTFE film as a triboelectric layer. Slider: (i) Cut a rectangle acrylic sheet as the substrate with dimensions of 3 cm (length) by 1 cm (width) by 5 mm (thickness) using a laser cutter. (ii) Cut a rectangle copper foil as the FE with dimensions of 3 cm (length) by 9 mm (width) by 50 μm (thickness) and paste under the acrylic sheet. There is a gap of about 1 mm between the copper foil and the left end of the acrylic sheet. (iii) Cut a rectangle copper foil with dimensions of 3 cm (length) by 5 mm (width) by 50 μm (thickness) and paste on the left end of the acrylic sheet along the vertical direction with a small gap between the surface of the PTFE film and the copper foil. (iv) Both copper foils are connected by wires for electrical measurement.

Fabrication of the rotary mode DC-TENG

Rotator: (i) Cut a disc-shaped acrylic as the substrate using a laser cutter. The substrate has a diameter of 20 cm and a thickness of 3 mm. (ii) Drill a through-hole at the center of the substrate to connect to a commercial motor. (iii) Adhere a piece of foam on the surface of the substrate with the same size as the buffer. (iv) Paste a PTFE film, the same size as the triboelectric layer, on the surface of the foam. Stator: (i) Cut a disc-shaped acrylic sheet as the substrate (diameter, 20 cm; thickness, 3 mm) using a laser cutter. The substrate has a collection of radially arrayed sectors with a central angle of 3°. (ii) Adhere another commercial Printed Circuit Board (PCB) with the same shape and size as the substrate. The PCB has predeposited copper on one surface, and there is a gap of about 1 mm between the copper and the sector edge. The copper foils are mutually connected at one end as an FE. (iii) Cut many rectangle copper foils with dimensions of 5 cm (length) by 5 mm (width) by 50 μm (thickness) and paste them at the left sector edge of the substrate along the vertical direction with a small gap between the surface of the PTFE film and the copper foils. All the copper foils are connected together as a CCE. (iv) Both electrodes are connected by wires for electrical measurement.

Electrical measurement and characterization

The sliding process was implemented by a linear motor (TSMV120-1S). The rotary process was driven by a commercial motor (80BL165S75-3130TK0). A programmable electrometer (Keithley Instruments model 6514) was adopted to measure the short-circuit current and transferred charges of the DC-TENG. A mixed domain oscilloscope (MDO3024) was used to test the open-circuit voltage of the DC-TENG. The surface potential of PTFE was tested by using an Isoprobe electrostatic voltmeter (model 279). Humidity was monitored by a commercial humidity sensor. A potentiostat (Bio-Logic VSP-300, France) was used to test the capacitance of the capacitor and the charging/discharging curves of the self-charging power system.

Downloaded from http://advances.sciencemag.org/ on March 31, 2021

SUPPLEMENTARY MATERIALS

Supplementary material for this article is available at http://advances.sciencemag.org/cgi/content/full/5/4/eaav6437/DC1

Supplementary Materials and Methods
Fig. S1. Working principle of the sliding mode DC-TENG during the first cycle.
Fig. S2. Working mechanism of a conventional sliding TENG.
Fig. S3. Equivalent circuit model of a conventional TENG.
Fig. S4. Surface potential of the PTFE film under different conditions.
Fig. S5. Transferred charges of the sliding mode DC-TENG at different velocities.
Fig. S6. Output performance of the sliding mode DC-TENG where the triboelectric materials are PTFE and nitrile.
Fig. S7. Charge density of the sliding mode DC-TENG with nanostructured PTFE.
Fig. S8. Short-circuit current of the sliding mode DC-TENG at different gap.
Fig. S9. Working mechanism of the sliding mode DC-TENG with two CCEs at the two ends of the slider.
Fig. S10. Output performance of the sliding mode DC-TENG with two electrodes at the two ends of the slider.
Fig. S11. Output performance of the DC-TENG with different FE widths.
Fig. S12. Output performance of the DC-TENG in parallel.
Fig. S13. Output performance of the DC-TENG with different CCE lengths.
Fig. S14. Long-term output current of the sliding mode DC-TENG.
Fig. S15. Average charge at different rotation rates when the rotary motor rotates stably.
Table S1. Charge density of a conventional sliding TENG and our sliding DC-TENG.
Table S2. Crest factor of the rotary mode DC-TENG at different rotation rates.
Table S3. Average charge and the average value of steady current at different rotation rates.
Note S1. Working principle of the sliding mode DC-TENG during the first cycle.
Note S2. Working mechanism and equivalent circuit model of a conventional sliding TENG.
Note S3. Short-circuit current of the DC-TENG at different gap.
Note S4. Output performance of the sliding mode DC-TENG with two CCEs at the two ends of the slider.
Note S5. Short-circuit current of the DC-TENG with different FE widths.
Note S6. Calculation of the crest factor and average current.
Note S7. Calculation of the equivalent input current of an electronic watch.
Movie S1. An electronic watch is powered directly by the sliding mode DC-TENG.
Movie S2. An electronic calculator is powered by the rotary mode DC-TENG.
Movie S3. LEDs are powered by the rotary mode DC-TENG.
References (*37*–*39*)

REFERENCES AND NOTES

1. L. E. Bell, Cooling, heating, generating power, and recovering waste heat with thermoelectric systems. *Science* **321**, 1457–1461 (2008).
2. S. Chu, A. Majumdar, Opportunities and challenges for a sustainable energy future. *Nature* **488**, 294–303 (2012).
3. M. K. Debe, Electrocatalyst approaches and challenges for automotive fuel cells. *Nature* **486**, 43–51 (2012).
4. X. Wang, J. Song, J. Liu, Z. L. Wang, Direct-current nanogenerator driven by ultrasonic waves. *Science* **316**, 102–105 (2007).
5. Z. L. Wang, J. Song, Piezoelectric nanogenerators based on zinc oxide nanowire arrays. *Science* **312**, 242–246 (2006).
6. X. Pu, H. Guo, J. Chen, X. Wang, Y. Xi, C. Hu, Z. L. Wang, Eye motion triggered self-powered mechnosensational communication system using triboelectric nanogenerator. *Sci. Adv.* **3**, e1700694 (2017).
7. F. Yi, X. Wang, S. Niu, S. Li, Y. Yin, K. Dai, G. Zhang, L. Lin, Z. Wen, H. Guo, J. Wang, M.-H. Yeh, Y. Zi, Q. Liao, Z. You, Y. Zhang, Z. L. Wang, A highly shape-adaptive, stretchable design based on conductive liquid for energy harvesting and self-powered biomechanical monitoring. *Sci. Adv.* **2**, e1501624 (2016).
8. Z. Wen, M.-H. Yeh, H. Guo, J. Wang, Y. Zi, W. Xu, J. Deng, L. Zhu, X. Wang, C. Hu, L. Zhu, X. Sun, Z. L. Wang, Self-powered textile for wearable electronics by hybridizing fibershaped nanogenerators, solar cells, and supercapacitors. *Sci. Adv.* **2**, e1600097 (2016).
9. C. Wu, W. Ding, R. Liu, J. Wang, A. C. Wang, J. Wang, S. Li, Y. Zi, Z. L. Wang, Keystroke dynamics enabled authentication and identification using triboelectric nanogenerator array. *Mater. Today* **21**, 216–222 (2018).
10. M. El-hami, P. Glynne-Jones, N. M. White, M. Hill, S. Beeby, E. James, A. D. Brown, J. N. Ross, Design and fabrication of a new vibration-based electromechanical power generator. *Sens. Actuators A Phys.* **92**, 335–342 (2001).
11. S. P. Beeby, R. N. Torah, M. J. Tudor, P. Glynne-Jones, T. O'Donnell, C. R. Saha, S. Roy, A micro electromagnetic generator for vibration energy harvesting. *J. Micromech. Microeng.* **17**, 1257–1265 (2007).
12. R. Yang, Y. Qin, L. Dai, Z. L. Wang, Power generation with laterally packaged piezoelectric fine wires. *Nat. Nanotechnol.* **4**, 34–39 (2009).
13. G.-T. Hwang, Y. Kim, J.-H. Lee, S. Oh, C. K. Jeong, D. Y. Park, J. Ryu, H. Kwon, S.-G. Lee, B. Joung, D. Kim, K. J. Lee, Self-powered deep brain stimulation *via* a flexible PIMNT energy harvester. *Energy Environ. Sci.* **8**, 2677–2684 (2015).
14. Z. L. Wang, Triboelectric nanogenerators as new energy technology for self-powered systems and as active mechanical and chemical sensors. *ACS Nano* **7**, 9533–9557 (2013).
15. H. Guo, X. Pu, J. Chen, Y. Meng, M.-H. Yeh, G. Liu, Q. Tang, B. Chen, D. Liu, S. Qi, C. Wu, C. Hu, J. Wang, Z. L. Wang, A highly sensitive, self-powered triboelectric auditory sensor for social robotics and hearing aids. *Sci. Robot.* **3**, eaat2516 (2018).
16. C. Dagdeviren, Z. Li, Z. L. Wang, Energy harvesting from the animal/human body for self-powered electronics. *Annu. Rev. Biomed. Eng.* **19**, 85–108 (2017).
17. G.-T. Hwang, J. Yang, S. H. Yang, H.-Y. Lee, M. Lee, D. Y. Park, J. H. Han, S. J. Lee, C. K. Jeong, J. Kim, K.-I. Park, K. J. Lee, A reconfigurable rectified flexible energy harvester via solid-state single crystal grown PMN-PZT. *Adv. Energy Mater.* **5**, 1500051 (2015).
18. F.-R. Fan, Z.-Q. Tian, Z. L. Wang, Flexible triboelectric generator. *Nano Energy* **1**, 328–334 (2012).
19. J. Chen, Y. Huang, N. Zhang, H. Zou, R. Liu, C. Tao, X. Fan, Z. L. Wang, Micro-cable structured textile for simultaneously harvesting solar and mechanical energy. *Nat. Energy* **1**, 16138 (2016).
20. J. Wang, X. Li, Y. Zi, S. Wang, Z. Li, L. Zheng, F. Yi, S. Li, Z. L. Wang, A flexible fiber-based supercapacitor–triboelectric-nanogenerator power system for wearable electronics. *Adv. Mater.* **27**, 4830–4836 (2015).
21. Y. Zi, H. Guo, Z. Wen, M.-H. Yeh, C. Hu, Z. L. Wang, Harvesting low-frequency (<5 Hz) irregular mechanical energy: A possible killer application of triboelectric nanogenerator. *ACS Nano* **10**, 4797–4805 (2016).
22. G. Zhu, J. Chen, T. Zhang, Q. Jing, Z. L. Wang, Radial-arrayed rotary electrification for high performance triboelectric generator. *Nat. Commun.* **5**, 3426 (2014).
23. Q. Jing, Y. Xie, G. Zhu, R. P. S. Han, Z. L. Wang, Self-powered thin-film motion vector sensor. *Nat. Commun.* **6**, 8031 (2015).
24. S. Wang, L. Lin, Z. L. Wang, Triboelectric nanogenerators as self-powered active sensors. *Nano Energy* **11**, 436–462 (2015).
25. B. Meng, W. Tang, Z.-h. Too, X. Zhang, M. Han, W. Liu, H. Zhang, A transparent single-friction-surface triboelectric generator and self-powered touch sensor. *Energy Environ. Sci.* **6**, 3235–3240 (2013).
26. H. S. Wang, C. K. Jeong, M.-H. Seo, D. J. Joe, J. H. Han, J.-B. Yoon, K. J. Lee, Performance-enhanced triboelectric nanogenerator enabled by wafer-scale nanogrates of multistep pattern downscaling. *Nano Energy* **35**, 415–423 (2017).
27. C. Zhang, T. Zhou, W. Tang, C. Han, L. Zhang, Z. L. Wang, Rotating-disk-based direct-current triboelectric nanogenerator. *Adv. Energy Mater.* **4**, 1301798 (2014).
28. Y. Yang, H. Zhang, Z. L. Wang, Direct-current triboelectric generator. *Adv. Funct. Mater.* **24**, 3745–3750 (2014).
29. H. Ryu, J. H. Lee, U. Khan, S. S. Kwak, R. Hinchet, S.-W. Kim, Sustainable direct current powering a triboelectric nanogenerator *via* a novel asymmetrical design. *Energy Environ. Sci.* **11**, 2057–2063 (2018).
30. X. X. Zhu, Z. B. Li, X. S. Li, L. Su, X. Y. Wei, S. Y. Kuang, B. W. Su, J. Yang, Z. L. Wang, G. Zhu, Triboelectrification-enabled thin-film tactile matrix for self-powered high-resolution imaging. *Nano Energy* **50**, 497–503 (2018).
31. J. Liu, A. Goswami, K. Jiang, F. Khan, S. Kim, R. McGee, Z. Li, Z. Hu, J. Lee, T. Thundat, Direct-current triboelectricity generation by a sliding Schottky nanocontact on MoS_2 multilayers. *Nat. Nanotechnol.* **13**, 112–116 (2018).
32. Y. Zi, S. Niu, J. Wang, Z. Wen, W. Tang, Z. L. Wang, Standards and figure-of-merits for quantifying the performance of triboelectric nanogenerators. *Nat. Commun.* **6**, 8376 (2015).
33. S. Wang, Y. Xie, S. Niu, L. Lin, C. Liu, Y. S. Zhou, Z. L. Wang, Maximum surface charge density for triboelectric nanogenerators achieved by ionized-air injection: Methodology and theoretical understanding. *Adv. Mater.* **26**, 6720–6728 (2014).
34. J. Chun, B. U. Ye, J. W. Lee, D. Choi, C.-Y. Kang, S.-W. Kim, Z. L. Wang, J. M. Baik, Boosted output performance of triboelectric nanogenerator via electric double layer effect. *Nat. Commun.* **7**, 12985 (2016).
35. J. Wang, S. Li, F. Yi, Y. Zi, J. Lin, X. Wang, Y. Xu, Z. L. Wang, Sustainably powering wearable electronics solely by biomechanical energy. *Nat. Commun.* **7**, 12744 (2016).
36. J. Wang, C. Wu, Y. Dai, Z. Zhao, A. Wang, T. Zhang, Z. L. Wang, Achieving ultrahigh triboelectric charge density for efficient energy harvesting. *Nat. Commun.* **8**, 88 (2017).
37. S. Wang, L. Lin, Y. Xie, Q. Jing, S. Niu, Z. L. Wang, Sliding-triboelectric nanogenerators based on in-plane charge-separation mechanism. *Nano Lett.* **13**, 2226–2233 (2013).
38. S. Niu, S. Wang, L. Lin, Y. Liu, Y. S. Zhou, Y. Hu, Z. L. Wang, Theoretical study of contact-mode triboelectric nanogenerators as an effective power source. *Energy Environ. Sci.* **6**, 3576–3583 (2013).
39. S. Niu, Y. S. Zhou, S. Wang, Y. Liu, L. Lin, Y. Bando, Z. L. Wang, Simulation method for optimizing the performance of an integrated triboelectric nanogenerator energy harvesting system. *Nano Energy* **8**, 150–156 (2014).

Downloaded from http://advances.sciencemag.org/ on March 31, 2021

Acknowledgments
Funding: This research was supported by the National Key R&D Program from the Minister of Science and Technology (2016YFA0202704), the Beijing Municipal Science and Technology Commission (Z171100000317001, Z171100002017017, and Y3993113DF), and the National Natural Science Foundation of China (grant nos. 61774016, 51432005, 5151101243, and 51561145021). Patents have been filed based on the research results presented in this manuscript. **Author contributions:** D.L., X.Y., H.G., J.W., and Z.L.W. conceived the idea, analyzed the data, and wrote the paper. D.L. and H.G. designed the materials of the TENGs. D.L., X.Y., and J.W. optimized the structure of the TENGs. L.Z., X.L., and C.Z. helped with the experiments. All the authors discussed the results and commented on the manuscript. **Competing interests:** J.W., D.L., and X.Y. are inventors on a patent related to this work that is currently under review with the State Intellectual Property Office of P. R. China (serial no. 201811362862.3, 15 November 2018). The other authors declare that they have no competing interests. **Data and materials availability:** All data needed to evaluate the conclusions in the paper are present in the paper and/or the Supplementary Materials. Additional data related to this paper may be requested from the authors.

Submitted 8 October 2018
Accepted 13 February 2019
Published 5 April 2019
10.1126/sciadv.aav6437

Citation: D. Liu, X. Yin, H. Guo, L. Zhou, X. Li, C. Zhang, J. Wang, Z. L. Wang, A constant current triboelectric nanogenerator arising from electrostatic breakdown. *Sci. Adv.* **5**, eaav6437 (2019).

Downloaded from http://advances.sciencemag.org/ on March 31, 2021

Science Advances

A constant current triboelectric nanogenerator arising from electrostatic breakdown

Di Liu, Xing Yin, Hengyu Guo, Linglin Zhou, Xinyuan Li, Chunlei Zhang, Jie Wang and Zhong Lin Wang

Sci Adv **5** (4), eaav6437.
DOI: 10.1126/sciadv.aav6437

ARTICLE TOOLS http://advances.sciencemag.org/content/5/4/eaav6437

SUPPLEMENTARY MATERIALS http://advances.sciencemag.org/content/suppl/2019/04/01/5.4.eaav6437.DC1

REFERENCES This article cites 39 articles, 6 of which you can access for free
http://advances.sciencemag.org/content/5/4/eaav6437#BIBL

PERMISSIONS http://www.sciencemag.org/help/reprints-and-permissions

Use of this article is subject to the Terms of Service

Science Advances (ISSN 2375-2548) is published by the American Association for the Advancement of Science, 1200 New York Avenue NW, Washington, DC 20005. The title *Science Advances* is a registered trademark of AAAS.

Copyright © 2019 The Authors, some rights reserved; exclusive licensee American Association for the Advancement of Science. No claim to original U.S. Government Works. Distributed under a Creative Commons Attribution NonCommercial License 4.0 (CC BY-NC).

Downloaded from http://advances.sciencemag.org/ on March 31, 2021